

Space and Time Adaptive Two-Mesh *hp*-FEM for Transient Microwave Heating Problems

L. Dubcova², P. Solin^{1,2}, J. Cerveny², P. Kus²

¹University of Nevada, Reno, USA

²Institute of Thermomechanics, Prague, Czech Republic

Abstract

We propose a novel, highly efficient and accurate space and time adaptive higher-order finite element method (*hp*-FEM) for evolutionary microwave heating problems. Since the electric field \mathbf{E} and temperature field T are very different in nature, we approximate them on individual meshes that change dynamically in time independently of each other. Although the approximations of \mathbf{E} and T are defined on different meshes, the coupling is treated in a monolithic fashion using a complex-valued approximate temperature. We present numerical experiments showing that the novel method is clearly superior to its natural competitors – the space and time adaptive (single mesh) *hp*-FEM and the space and time adaptive two-mesh *h*-FEM. In all cases, comparisons in both the number of DOF (discrete problem size) and CPU time are presented. The methodology is freely available on-line in the form of a GPL-licensed C++/Python library Hermes¹.

¹<http://spilka.math.unr.edu/hermes/>.

1 Introduction

The effect of microwaves on the heating of materials was discovered in 1945 by Dr. Percy Spencer, research scientist at the Raytheon company. The first microwave oven the company built in 1947 was 1.8 m tall and weighed 340 kg. During the past two decades, the microwave oven has become a ubiquitous technology which, besides extensive household use, is employed in a variety of material processing technologies.

In physical terms, the electric field deposits energy into the heated object (load), which creates internal heat sources. The rising temperature of the load changes its material parameters and in turn also the original electric field. In this paper we study a model consisting of the time-harmonic Maxwell's equation and the transient heat transfer equation, which are coupled both-ways through the heat sources term and material parameters of the load in a nonlinear way.

The most widely used numerical method for the computer simulation of microwave heating (and other problems in material and food processing) is the finite difference time-domain (FDTD) method [6, 8]. The FDTD method is a grid-based differential time-domain numerical method, where space and time partial derivatives are discretized using central-difference approximations. The main advantage of the FDTD is the simplicity of software implementation. The FDTD is sometimes combined with the finite volume method (FV) [6] or finite element method (FEM) [7] for the thermal part of

the problem. In contrast to FDTD, FEM allows for variable element sizes, it is capable of higher accuracy, and better suited to handle irregular geometries. Probably the first papers using FEM for the simulation of a microwave heating problem were [12, 13].

During the last decade, significant progress was made in adaptive higher-order finite element methods (*hp*-FEM) for second-order elliptic equations and time-harmonic Maxwell's equations (see, e.g., [1, 4, 5, 14, 16, 17] and the references therein). Adaptive *hp*-FEM is known to achieve extremely fast (typically exponential) convergence rates by optimally combining finite elements of different sizes (h) and polynomial degrees (p). Recently, adaptive *hp*-FEM was extended to the multiphysics coupled problem of stationary linear thermoelasticity [15].

In thermoelasticity, the gradient of the displacement field typically is singular at re-entrant corners and large amounts of local refinements are required to resolve the corresponding stress intensity factors with sufficient accuracy. In contrast to that, the temperature field is smooth everywhere in the domain, and thus extra refinements at re-entrant corners are not necessary. It was demonstrated in [15] that since the interacting physical fields had such significant qualitative differences, it was advantageous to approximate them on different meshes equipped with independent adaptivity mechanisms. A novel multimesh *hp*-FEM was introduced to avoid operator splitting and preserve the coupling structure of the problem when working with multiple meshes.

The electrical field \mathbf{E} and the temperature T participating in the microwave heating exhibit significant qualitative differences as well: The electric field typically is singular at sharp corners while the temperature field remains smooth everywhere in the domain. Vice versa, the temperature contains a thin layer of very steep gradients in the vicinity of the heated object, which is not found in the electric field. In order to resolve both fields with sufficient accuracy, one usually needs to apply substantial amounts of local refinements both in the vicinity of the corners and in the thermal layers.

Encouraged by the results of [15], in this paper we propose a novel adaptive hp -FEM that approximates the fields \mathbf{E} and T on individual meshes equipped with independent hp -adaptivity mechanisms. The meshes, moreover, change dynamically in time independently of each other as dictated by the corresponding error components in \mathbf{E} and T , respectively. The time step is adjusted adaptively using the so-called *PID controller* [18]. The Maxwell's equation is discretized using higher-order vector-valued $\mathbf{H}(\text{curl})$ elements (edge elements) [2, 10, 11] while standard continuous higher-order H^1 -elements are used to approximate the temperature. The coupling of the Maxwell's equation and the transient heat transfer equation is treated in a monolithic way, in the sense that the fields \mathbf{E} and T always are unknown simultaneously. We also present a novel technique of arbitrary-level hanging nodes that makes automatic hp -adaptivity very efficient by avoiding unwanted regularity enforced refinements.

The outline of the paper is as follows: In Section 2 we introduce a model

problem and formulate the underlying coupled transient PDE system along with the corresponding boundary and initial conditions. In Section 3 we employ the Rothe's method to approximate the transient PDE system with a series of spatial ones, and write their variational (weak) formulation. In this section we also discuss a suitable monolithic discretization strategy for the nonlinear PDE system on each time level, and explain the need for complex-valued approximate temperature. We present a novel adaptive two-mesh hp -FEM algorithm for the spatial problems, as well as a suitable controller for the time step size. Numerical examples comparing fixed and adaptive time stepping as well as various versions of the space and time adaptive algorithm are presented in Section 4. Conclusions and outlook are drawn in Section 5.

2 Model problem

We consider a two-dimensional domain depicted in Fig. 1, consisting of a square cavity attached to a square waveguide. The size of the domain is chosen so that the edge length of the waveguide is $L/2$, and the edge length of the cavity equals to $5L/2$, where $L = c/f$ is the length of the incoming waves. With standard frequency of microwave ovens, $f = 2.45$ GHz, the wavelength equals to 12.236 cm. A horizontal wave is generated via a prescribed time-harmonic current along the right edge of the waveguide (represented by a Neumann boundary condition). Other walls are perfect conductors.

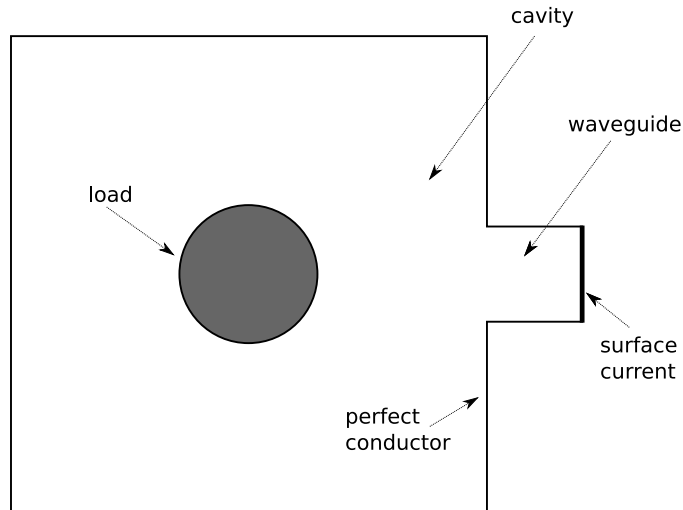


Figure 1: Microwave oven with a circular load.

The oven is filled with air. In the middle of the cavity is a circular load with temperature-dependent dielectric parameters (see Section 4).

2.1 Underlying coupled PDE system

The electromagnetic field is modeled via the time-harmonic Maxwell's equation

$$\nabla \times (\mu_r^{-1} \nabla \times \mathbf{E}) - i\gamma\kappa \sqrt{\frac{\mu_0}{\epsilon_0}} \mathbf{E} - \epsilon_r \kappa^2 \mathbf{E} = 0, \quad (1)$$

where $\mathbf{E} = \mathbf{E}(\mathbf{x}, t)$ is the (complex) vector-valued phasor of the harmonic electric field strength, $T = T(\mathbf{x}, t)$ the temperature, $\mu_r = \mu/\mu_0$ the relative magnetic permeability, $\kappa = \omega/c$ the wave number, i the imaginary unit, $\epsilon_r = \epsilon_r(\mathbf{x}, T) = \epsilon/\epsilon_0$ the relative electric permittivity, $\gamma = \gamma(\mathbf{x}, T)$ the electric conductivity, ω the angular frequency and c the speed of light in vacuum.

Note that ϵ_r and γ depend on \mathbf{x} and T . These parameters are different for the load and the air, and they are temperature-dependent for the load only.

The vector-valued surface current \mathbf{J}_s on the right edge of the waveguide is defined via a Neumann boundary condition

$$\mathbf{n} \times (\mu_r^{-1} \nabla \times \mathbf{E}) = i\omega \mathbf{J}_s, \quad (2)$$

and a perfect conductor boundary condition

$$\mathbf{E} \cdot \mathbf{t} = 0 \quad (3)$$

is used for the rest of the boundary.

The temperature field T is described by the heat-transfer equation

$$c_p \varrho \frac{\partial T}{\partial t} - k \Delta T = Q, \quad (4)$$

where c_p stands for the specific heat capacity, ϱ is the density and k the thermal conductivity. The right-hand side contains a heat source coming from the electric field,

$$Q = \frac{1}{2} \gamma |\mathbf{E}|^2.$$

Along the oven boundary we define a Newton boundary condition

$$\frac{\partial T}{\partial n} = \alpha(T - T_{env}), \quad (5)$$

where α is the heat transfer coefficient and T_{env} the external temperature. The initial condition for the temperature has the form

$$T_0 = T_{env}. \quad (6)$$

3 Space and time adaptive hp -FEM

We employ the classical *Rothe's method* [9] combined with our recent multimesh hp -FEM [15] to design a suitable space and time adaptive hp -FEM algorithm for the transient coupled PDE problem (1), (4). Let us begin with the discretization in time using a fixed time step $\tau > 0$ and postpone the discussion of adaptive time stepping to Paragraph 3.5. The approximations of \mathbf{E} and T on the time level t_n are denoted by \mathbf{E}^n and T^n , respectively. By replacing in (4) the time-derivative with a backward time difference

$$\frac{\partial T}{\partial t} \approx \frac{T^n - T^{n-1}}{\tau},$$

we obtain

$$c_p \varrho \frac{T^n - T^{n-1}}{\tau} - k \Delta T^n = \frac{1}{2} \gamma(T^n) |\mathbf{E}^n|^2,$$

which yields an equation for T^n in the form

$$-k \Delta T^n + \frac{c_p \varrho}{\tau} T^n - \frac{1}{2} \gamma(T^n) |\mathbf{E}^n|^2 = \frac{c_p \varrho}{\tau} T^{n-1}. \quad (7)$$

Obviously, we are not limited to the first-order accurate implicit Euler method. For example, with a second-order accurate implicit backward difference formula

$$\frac{\partial T}{\partial t} \approx \frac{3T^n - 4T^{n-1} + T^{n-2}}{2\tau},$$

(4) translates into

$$-k \Delta T^n + \frac{3c_p \varrho}{2\tau} T^n - \frac{1}{2} \gamma(T^n) |\mathbf{E}^n|^2 = \frac{2c_p \varrho}{\tau} T^{n-1} - \frac{c_p \varrho}{2\tau} T^{n-2}. \quad (8)$$

The Maxwell's equation (1) now has the form

$$\nabla \times (\mu_r^{-1} \nabla \times \mathbf{E}^n) - i\gamma(T^n) \kappa \sqrt{\frac{\mu_0}{\epsilon_0}} \mathbf{E}^n - \epsilon_r(T^n) \kappa^2 \mathbf{E}^n = 0. \quad (9)$$

The system (7), (9) is still nonlinear, but it *no longer depends on time*. Thus in every time step we can solve it efficiently using adaptive *hp*-FEM in space.

Note that the right-hand sides of both (7) and (8) contain approximations T^{n-2} and/or T^{n-1} from the previous time levels, which are defined *on different locally refined meshes*. The shape of these meshes is not known a-priori since they are obtained as a result of an automatic adaptive process. Thus assembling over different meshes is necessary to solve adaptively equations arising in the Rothe's method. This can be done efficiently via a novel multimesh *hp*-FEM [15] which will be described briefly in Paragraph 3.2.

3.1 Weak formulation of system (7), (9)

Let us now state the variational (weak) formulation of the coupled problem (7), (9) for the purpose of finite element approximation: We are looking for a pair $(\mathbf{E}^n, T^n) \in \mathbf{Q} \times V$ such that

$$\begin{aligned} \int_{\Omega} \mu_r^{-1} (\nabla \times \mathbf{E}^n) \cdot (\nabla \times \overline{\mathbf{F}}) \, d\mathbf{x} - \int_{\Omega} \left(i\gamma(T^n) \kappa \sqrt{\frac{\mu_0}{\epsilon_0}} + \kappa^2 \epsilon_r(T^n) \right) \mathbf{E}^n \cdot \overline{\mathbf{F}} \, d\mathbf{x} \\ = \int_{\Gamma_1} i\omega \mathbf{J}_s \cdot \overline{\mathbf{F}} \, d\mathbf{S} \quad \text{for all } \mathbf{F} \in \mathbf{Q} \end{aligned} \quad (10)$$

and

$$\begin{aligned} \int_{\Omega} c_p \varrho T^n v \, d\mathbf{x} + \int_{\Omega} \tau k \nabla T^n \cdot \nabla v \, d\mathbf{x} + \int_{\partial\Omega} \tau \alpha T^n v \, d\mathbf{S} \\ - \int_{\Omega} \frac{\tau}{2} \gamma(T^n) |\mathbf{E}^n|^2 v \, d\mathbf{x} = \int_{\Omega} c_p \varrho T^{n-1} v \, d\mathbf{x} + \int_{\partial\Omega} \tau \alpha T_{env} v \, d\mathbf{S} \end{aligned} \quad (11)$$

for all $v \in V$.

Above, $\mathbf{Q} = \{\mathbf{E} \in \mathbf{H}(\text{curl}, \Omega); \mathbf{E} \cdot \mathbf{t} = 0 \text{ on } \partial\Omega\}$, $V = H^1(\Omega)$, and $\overline{\mathbf{F}}$ stands for the complex-conjugate to \mathbf{F} .

3.2 Multimesh hp -FEM for system (10), (11)

In standard hp -FEM, the domain Ω is covered with a finite element mesh \mathcal{T} consisting of non-overlapping convex elements K_1, K_2, \dots, K_M (in practice usually triangles or quadrilaterals) equipped with polynomial degrees

$1 \leq p_1, p_2, \dots, p_M$. For reasons explained in Section 1, we prefer to approximate the fields \mathbf{E} and T on different meshes $\mathcal{T}_E = \{K_1, K_2, \dots, K_{M_1}\}$ and $\mathcal{T}_T = \{\tilde{K}_1, \tilde{K}_2, \dots, \tilde{K}_{M_2}\}$. The elements in both meshes have nonuniform polynomial degrees $p(K_i) = p_i$ and $p(\tilde{K}_j) = \tilde{p}_j$. In order to keep the algorithms on a reasonable level of complexity, for every problem we introduce a very coarse *master mesh* \mathcal{T}_m which is the same for both \mathbf{E} and T . Each of the meshes \mathcal{T}_E and \mathcal{T}_T is then arbitrary up to the condition that it is obtained from \mathcal{T}_m using some sequence of local refinements. The refinement sequences for \mathcal{T}_E and \mathcal{T}_T are mutually independent.

The stiffness matrix is assembled on a *virtual union mesh* \mathcal{T}_u which is the geometrical union of the meshes \mathcal{T}_E and \mathcal{T}_T (imagine printing the meshes on transparencies and putting them on each other). The union mesh \mathcal{T}_u is never constructed in the computer, but its virtual elements are traversed by the element-by-element assembling procedure analogously to the standard *hp*-FEM [17]. In practice, the meshes \mathcal{T}_E and \mathcal{T}_T can be very different, as we illustrate in Fig. 2.

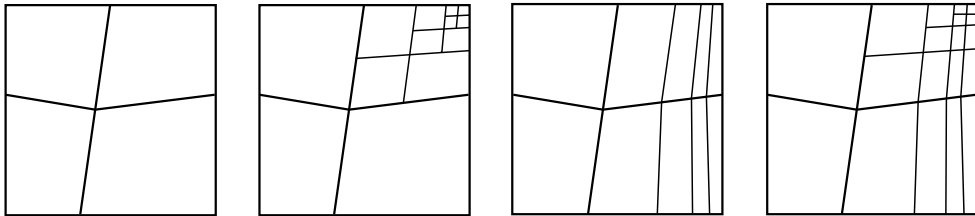


Figure 2: Sample master mesh \mathcal{T}_m (left), meshes \mathcal{T}_E and \mathcal{T}_T obtained by its independent refinements (middle), and the virtual union mesh \mathcal{T}_u (right).

The finite element problem is then formulated by restricting (10) and (11) to the finite-dimensional subspaces

$$\mathbf{Q}_{h,p} = \{\mathbf{E}_{h,p} \in \mathbf{Q}; \mathbf{E}_{h,p} \text{ is polynomial of degree } p_i \text{ in } K_i\} \subset \mathbf{Q},$$

$$V_{h,p} = \{T_{h,p} \in H^1(\Omega); T_{h,p} \text{ is polynomial of degree } \tilde{p}_j \text{ in } \tilde{K}_j\} \subset V.$$

3.3 Monolithic discretization and need for complex-valued temperature

In every time step, we linearize the equations (10), (11) using the approximations

$$\gamma(T^n)\mathbf{E}^n \approx \gamma(T_{k-1}^n)\mathbf{E}_k^n, \quad (12)$$

$$\epsilon_r(T^n)\mathbf{E}^n \approx \epsilon_r(T_{k-1}^n)\mathbf{E}_k^n, \quad (13)$$

$$\frac{\tau}{2}\gamma(T^n)|\mathbf{E}_k^n|^2 \approx \frac{\tau}{2}\gamma(T_{k-1}^n)\overline{\mathbf{E}_{k-1}^n} \cdot \mathbf{E}_k^n. \quad (14)$$

The initial values for the iteration in k are the values from the last time level: $T_0^n = T^{n-1}$ and $\mathbf{E}_0^n = \mathbf{E}^{n-1}$. If the material parameters $\gamma(T)$, $\epsilon_r(T)$ have steep derivatives in T or are discontinuous, or if τ is large, then it may be necessary to solve the linearized system (10), (11) for every $k = 1, 2, 3, \dots$ until the process converges. A suitable stopping criterion is a small relative

change between the approximations on the levels $k - 1$ and k ,

$$\frac{\|\mathbf{E}_k^n - \mathbf{E}_{k-1}^n\|_\Omega}{\|\mathbf{E}_k^n\|_\Omega} + \omega \frac{\|T_k^n - T_{k-1}^n\|_\Omega}{\|T_k^n\|_\Omega} < TOL,$$

where TOL is a user-defined constant and the meaning of ω will be described in Paragraph 3.4. Performing the iteration in k in every time step may be quite time-consuming. However, in most cases the material parameters $\gamma(T)$ and $\epsilon_r(T)$ change slowly with T and the time step τ is sufficiently small. Then it is enough to do just one step of the iterative process per time step (this is what we are doing in the numerical examples in Section 4).

It is worth mentioning that with the linearization (14), the approximate temperature $T_{h,p}$ becomes complex-valued. The reason is that while the nonlinear term $|\mathbf{E}_k^n|^2$ is real-valued, its linearization $\overline{\mathbf{E}_k^{n-1}} \cdot \mathbf{E}_k^n$ is not, and the presence of a complex-valued term in the linearized equation (11) makes $T_{h,p}$ complex-valued as well. However, in our experience, if \mathbf{E}_{k-1}^n and \mathbf{E}_k^n are close enough, then the imaginary part of $T_{h,p}$ is negligible (and it should go to zero quickly as $\mathbf{E}_k^n - \mathbf{E}_{k-1}^n \rightarrow \mathbf{0}$).

The linearization described above leads to the solution of complex-valued sparse systems of linear algebraic equations, which can be done using a suitable sparse direct solver. In practice, we usually employ UMFPACK [3].

3.4 Automatic hp -adaptivity

A major difference between automatic adaptivity in standard FEM (h -FEM) and in the hp -FEM is that an element with higher polynomial degree can be refined in many different ways. One can either increase its polynomial degree without spatial subdivision or the element can be split into 4 or 2 subelements with various distributions of polynomial degrees in the subelements. Fig. 3 illustrates this for a quartic quadrilateral element:

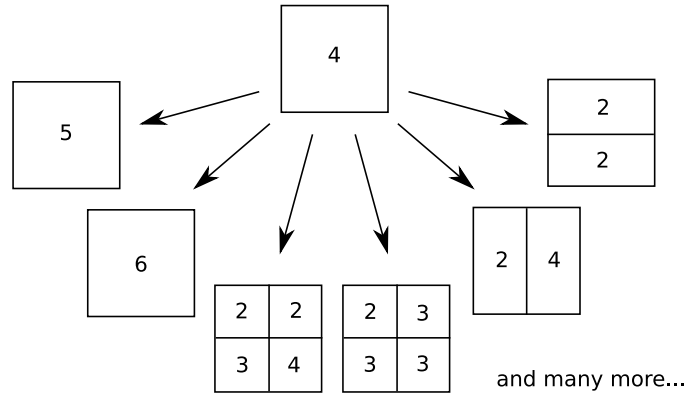


Figure 3: Multiple element refinement options in adaptive hp -FEM.

This means that traditional error estimates (that give one number per element) do not provide enough information to guide hp -adaptivity. In order to select an optimal refinement candidate, one needs to use some information *about the shape* of the error function $\mathbf{E}_{exact} - \mathbf{E}_{h,p}$. In principle, this information could be recovered from suitable estimates of higher derivatives of the solution, but such approach is not very practical and we are not aware of anyone who would be using it. We prefer to estimate the error by means

of the so-called *reference solutions* [5]. In practice, the reference solution $\mathbf{E}_{h,p}^{ref}$ is sought in an enriched finite element space $\mathbf{Q}_{h,p}^{ref} = \mathbf{Q}_{h/2,p+1}$, thus the difference $\mathbf{E}_{h,p}^{ref} - \mathbf{E}_{h,p}$ provides a sufficient information about the shape of the error of $\mathbf{E}_{h,p}$. Analogously, the shape of the error of $T_{h,p}$ (which is approximated using a different mesh) is estimated as $T_{h,p}^{ref} - T_{h,p}$. An outline of the adaptive algorithm is as follows:

1. Calculate the approximation pair $\mathbf{E}_{h,p}, T_{h,p}$ on the current meshes $\mathcal{T}_E, \mathcal{T}_T$ and the reference solution pair $\mathbf{E}_{h,p}^{ref}, T_{h,p}^{ref}$ on globally refined meshes $\mathcal{T}_E^{ref}, \mathcal{T}_T^{ref}$, respectively.
2. Calculate the relative error contribution

$$\frac{\|\mathbf{E}_{h,p}^{ref} - \mathbf{E}_{h,p}\|_{K_i}}{\|\mathbf{E}_{h,p}^{ref}\|_{\Omega}} \quad (15)$$

in each element $K_i \in \mathcal{T}_E$ in the $\mathbf{H}(\text{curl})$ -norm, a weighted relative error contribution

$$\omega \frac{\|T_{h,p}^{ref} - T_{h,p}\|_{\tilde{K}_j}}{\|T_{h,p}^{ref}\|_{\Omega}} \quad (16)$$

in each element $\tilde{K}_j \in \mathcal{T}_T$ in the H^1 -norm, and an estimate of the total approximation error in the norm

$$\mathcal{E}_{h,p} = \frac{\|\mathbf{E}_{h,p}^{ref} - \mathbf{E}_{h,p}\|}{\|\mathbf{E}_{h,p}^{ref}\|} + \omega \frac{\|T_{h,p}^{ref} - T_{h,p}\|}{\|T_{h,p}^{ref}\|}. \quad (17)$$

The user-defined parameter $\omega > 0$ in the relative error contribution

(16) and in the weighted global norm (17) can be used to change the balance in the overall accuracy of the resolution of the fields \mathbf{E} and T . The default value is $\omega = 1$.

3. Merge all elements of the meshes \mathcal{T}_E and \mathcal{T}_T into one list, sort them according to their error contributions (15), (16) and refine a user-defined part of them (for example 10%). Alternatively, keep refining until reaching a user-defined limit for the increase of the number of degrees of freedom (DOF) in one adaptivity step. Note: For each selected element, one needs to find the optimal hp -refinement candidate using the shape of the error function $\mathbf{E}_{h,p}^{ref} - \mathbf{E}_{h,p}$ (see [14] for details).
4. Repeat until the total error estimate (17) is below a user-defined tolerance.

3.5 Adaptive control of time step

Since the electric field \mathbf{E} and temperature T change in time unevenly, it is desirable to employ a time integration scheme enhanced with adaptive step size control. In this study we use the classical *proportional-integral-derivative (PID) controller* [18]. This method monitors the relative changes in $\mathbf{E}_{h,p}$ and $T_{h,p}$ between time steps as follows:

$$e_n = \max \left\{ \frac{\|\mathbf{E}_{h,p}^n - \mathbf{E}_{h,p}^{n-1}\|}{\|\mathbf{E}_{h,p}^n\|}, \frac{\|T_{h,p}^n - T_{h,p}^{n-1}\|}{\|T_{h,p}^n\|} \right\}. \quad (18)$$

The superscripts $n - 1$ and n stand for the solution at the previous and current time levels, respectively. If the value e_n is greater than a user-defined tolerance $\delta > 0$, then the PID controller discards the solution pair $\mathbf{E}_{h,p}^n, T_{h,p}^n$, and reduces the time step τ to

$$\tau_{new} = \frac{\delta}{e_n} \tau. \quad (19)$$

On the other hand, if $e_n < \delta$, then the time step is increased smoothly to

$$\tau_{new} = \left(\frac{e_{n-1}}{e_n} \right)^{k_P} \left(\frac{\delta}{e_n} \right)^{k_I} \left(\frac{e_{n-1}^2}{e_n e_{n-2}} \right)^{k_D} \tau. \quad (20)$$

We use the default values of the PID parameters as proposed in [18]:

$$k_P = 0.075, \quad k_I = 0.175, \quad k_D = 0.01.$$

4 Numerical examples

To illustrate the performance of the novel space and time adaptive hp -FEM algorithm, we solve the model problem from Section 2 with the following

parameters:

$$\begin{aligned}
 \epsilon_0 &= 8.8541878176 * 10^{-12} \text{ F/m}, & \mu_0 &= 1.256 * 10^{-6} \text{ N/A}^2, \\
 \epsilon_r &= 1.0 \text{ (air)}, & \gamma &= 0.0 \text{ S/m (air)}, \\
 \epsilon_r &= 0.05T + 6.8 \text{ (load)}, & \gamma &= 0.0005T + 0.03 \text{ S/m (load)}, \\
 f &= 2.45 \text{ GHz}, & J_s &= 0.001 \text{ mA}, \\
 \rho &= 1400 \text{ kg/m}^3, & c_p &= 7.532, \\
 k &= 0.025 \text{ W/(m K) (air)}, & k &= 0.3 \text{ W/(m K) (load)}.
 \end{aligned}$$

Notice that in this case both $\partial\gamma/\partial T$ and $\partial\epsilon_r/\partial T$ are very small. The external temperature (same as the initial temperature of the load) is $T_{env} = 20^\circ\text{C}$. The master mesh \mathcal{T}_m used as an initial mesh \mathcal{T}_E and \mathcal{T}_T in all following computations is shown in Fig. 4:

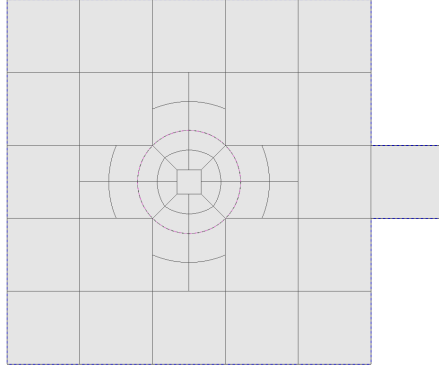


Figure 4: Master mesh \mathcal{T}_m , same for both \mathbf{E} and T .

In Figs. 5, 6 and 7 we show the approximations of $\mathbf{E}_{h,p}$ and $T_{h,p}$ along with the corresponding hp -meshes at three different time instants $t_1 = 2$ s, $t_2 = 5.5$ s and $t_3 = 10$ s. The meshes for $\mathbf{E}_{h,p}$ consist of vector-valued higher-order edge elements while the temperature meshes contain standard higher-order continuous elements. The greyscale colors and numbers in the elements indicate their polynomial degrees. Notice that the meshes \mathcal{T}_E and \mathcal{T}_T differ and that they change in time independently of each other.

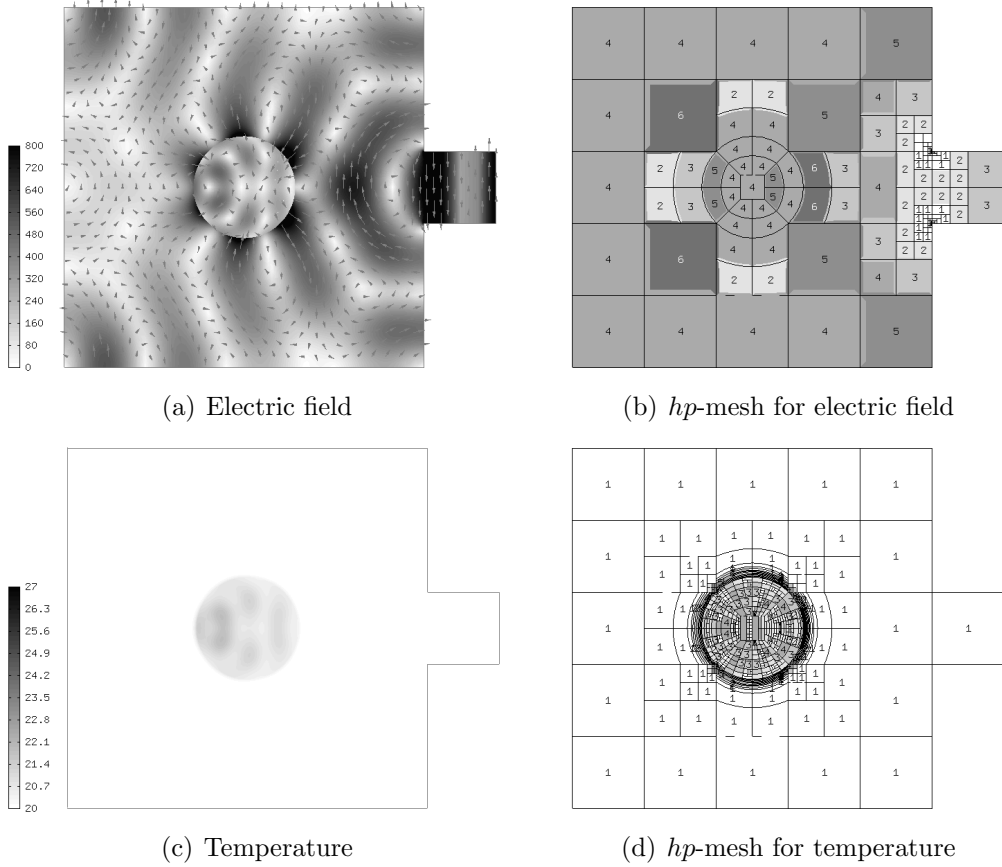


Figure 5: Electric field $\mathbf{E}_{h,p}$, temperature $T_{h,p}$ and the corresponding hp -meshes \mathcal{T}_E and \mathcal{T}_T at time $t_1 = 2$ s.

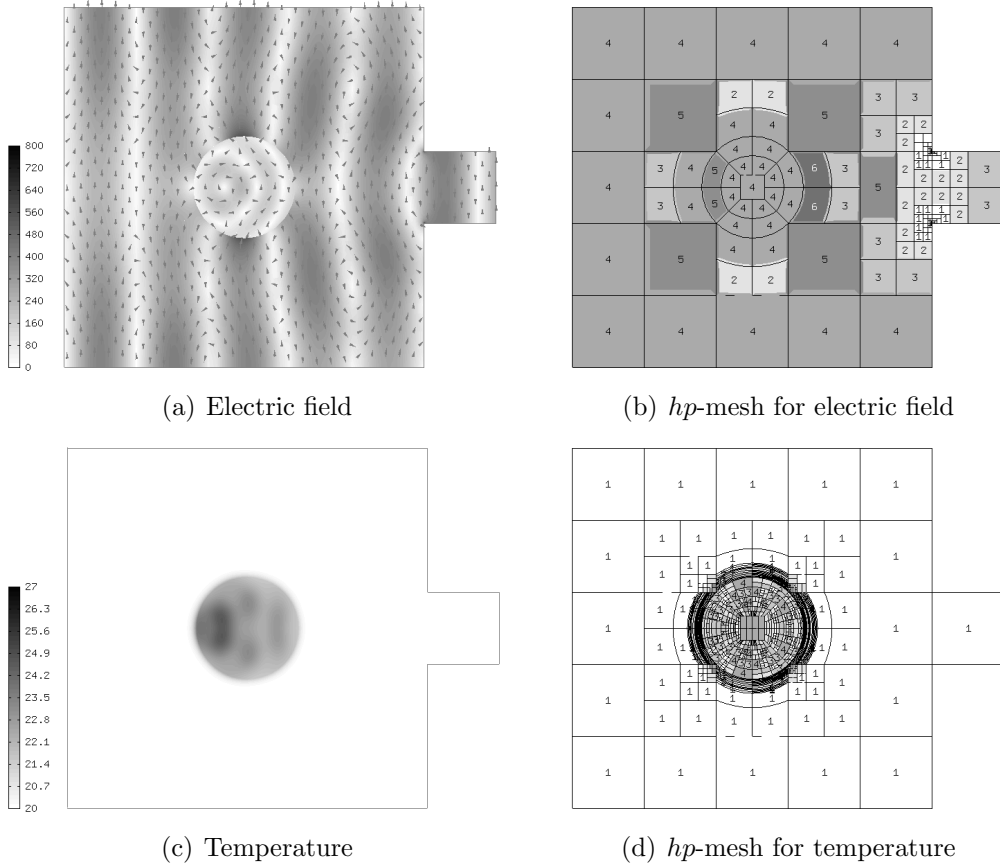


Figure 6: Electric field $\mathbf{E}_{h,p}$, temperature $T_{h,p}$ and the corresponding hp -meshes \mathcal{T}_E and \mathcal{T}_T at time $t_2 = 5.5$ s.

Note that in all Figs. 5, 6 and 7 the meshes for $\mathbf{E}_{h,p}$ are refined heavily in the vicinity of the sharp corners in order to capture the singularities while the meshes for $T_{h,p}$ remain very coarse there. Vice versa, the meshes for $T_{h,p}$ are very fine in the thermal layer surrounding the heated object while the meshes for $\mathbf{E}_{h,p}$ do not develop such refinements. Clearly, if both $\mathbf{E}_{h,p}$ and $T_{h,p}$ were approximated on the same mesh, then many temperature DOF would be wasted at the corners and many electric field DOF would be wasted

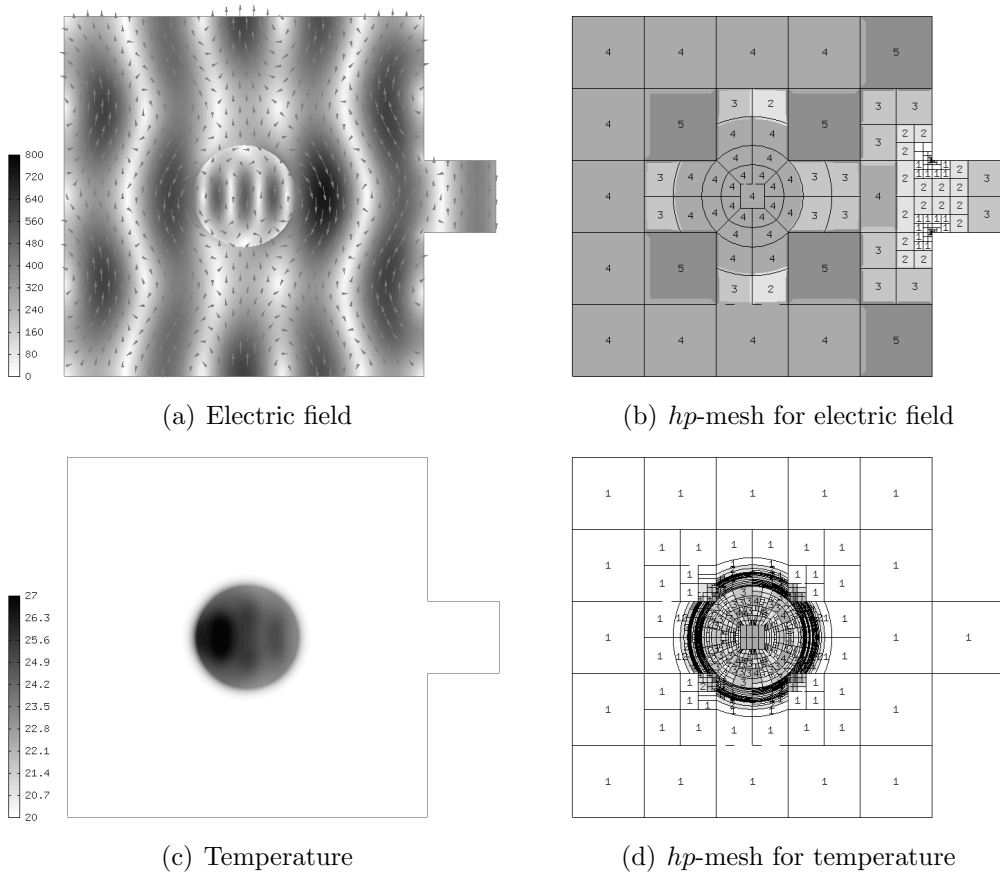


Figure 7: Electric field $\mathbf{E}_{h,p}$, temperature $T_{h,p}$ and the corresponding hp -meshes \mathcal{T}_E and \mathcal{T}_T at time $t_2 = 10$ s.

in the thermal layer region (a quantitative comparison will follow).

Comparing computations with a fixed and adaptive time step:

Fig. 8 shows how the time step τ changes through the computation if the PID controller is activated. The parameter δ in the controller is chosen to be $\delta = 2$.

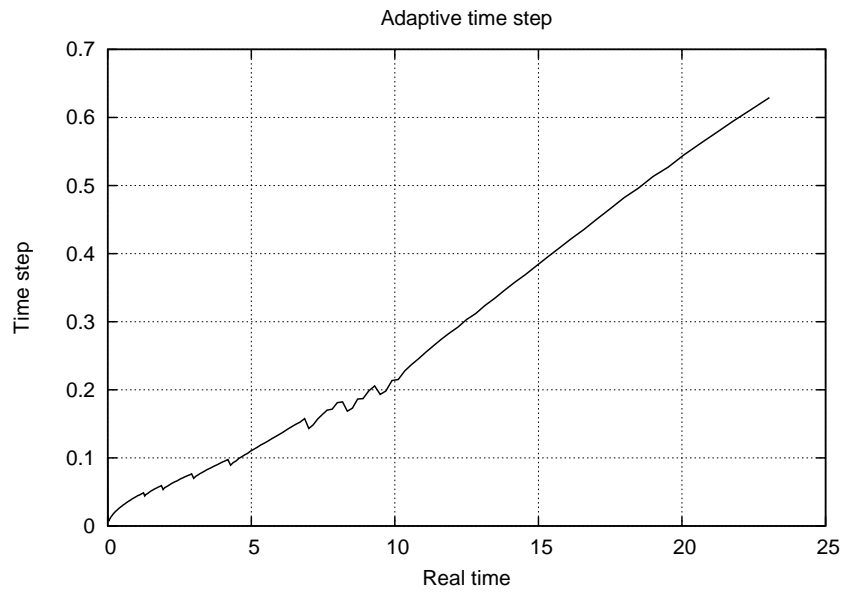


Figure 8: Size of the time step τ as a function of time.

Fig. 9 compares computations with a constant time step $\tau = 0.1$ s and with adaptive time step guided by the PID controller.

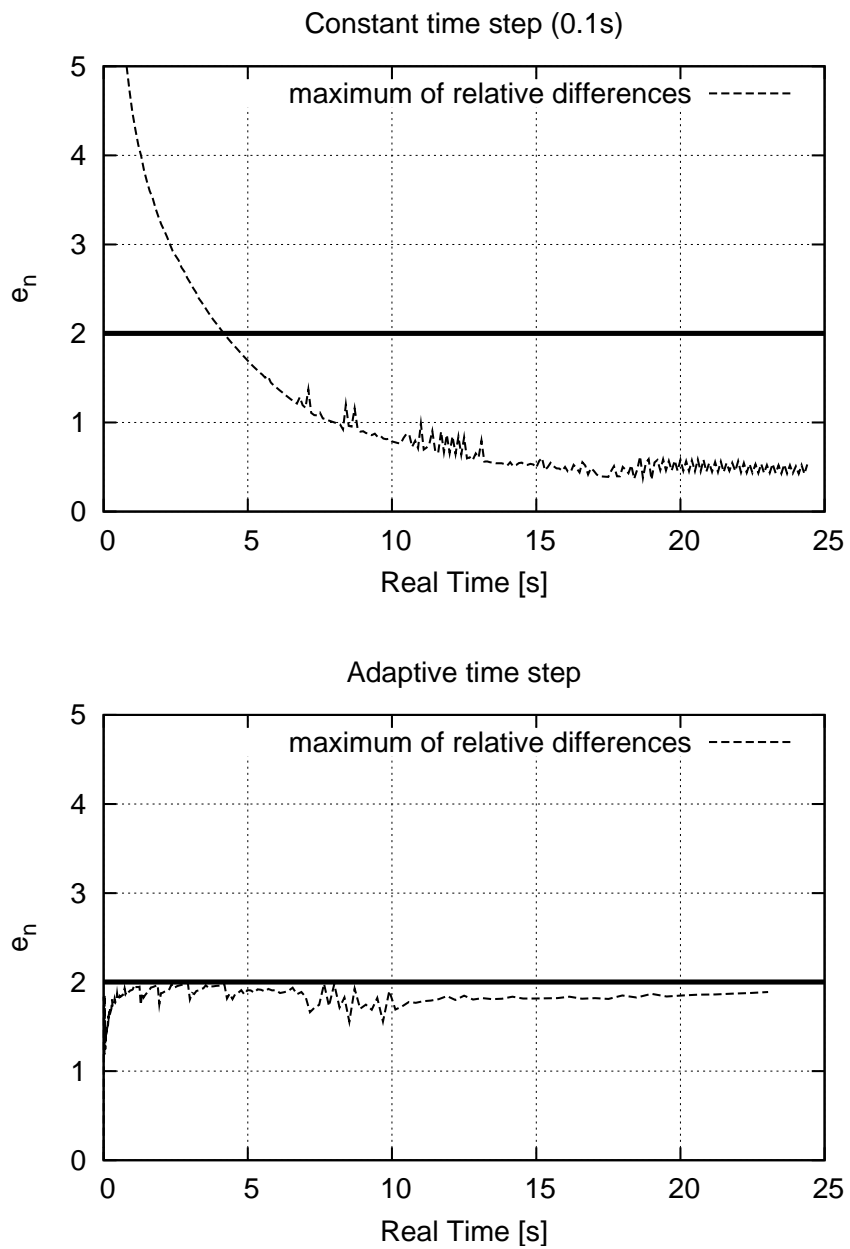


Figure 9: The value e_n used by the PID controller as a function of time for the fixed time step $\tau = 0.1$ s (top) and adaptive time step (bottom).

The reader can see in Fig. 9 that the time step τ is changing significantly in the time-adaptive case. At the beginning it is very small but it grows rapidly as time advances. It also follows from Fig.9 that the constant time step $\tau = 0.1$ s is too large during the first 5 seconds of heating, and then it becomes unnecessarily short for the remaining 20 seconds.

Multimesh hp -FEM vs. single-mesh hp -FEM and multimesh h -FEM, monolithic discretization:

Next we run the following computations:

- Adaptive single-mesh hp -FEM (with the same meshes for \mathbf{E} and T).
The meshes change dynamically in time (both in h and p) but remain the same for both \mathbf{E} and T all the time.
- Adaptive multimesh h -FEM with biquadratic elements for \mathbf{E} and bilinear elements for T . The meshes change dynamically in time independently of each other (only in h , not in p).

For fairness of comparison, we used the same level of accuracy for the adaptive process on each time level, the same value of parameter δ of the PID controller, and also all other parameters were the same. The results are presented in Figs. 10 and 11.

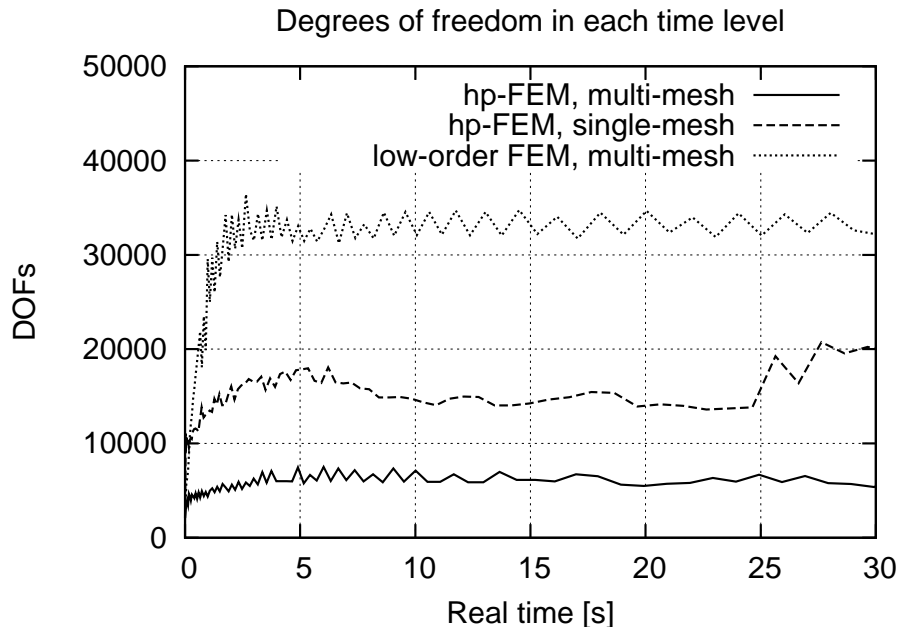


Figure 10: The number of DOF as the function of physical time (monolithically coupled discretization).

Fig. 10 shows that the multimesh hp -FEM consumed substantially fewer DOF than both other methods. The outcome of the comparison between the single-mesh hp -FEM and the multi-mesh h -FEM was hard to predict a priori and we find it very interesting. In this case, the single-mesh hp -FEM was more efficient than the multi-mesh h -FEM. However, we suspect that the comparison between these two methods might turn out differently in other problems, and we intend to analyze this subject in more detail later.

The differences in the number of DOF translate naturally into different CPU times, as shown in Fig. 11.

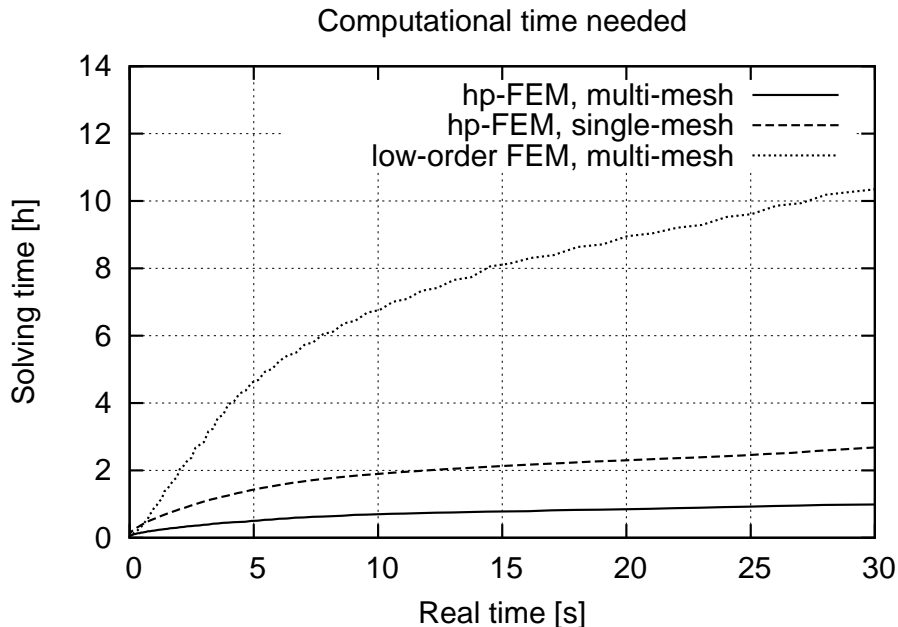


Figure 11: The CPU time of computation as the function of physical time (monolithically coupled discretization).

Fig. 11 shows that the CPU times consumed by the three methods are proportional to the number of DOF used: The multimesh hp -FEM was fastest, while the multi-mesh h -FEM with biquadratic elements for \mathbf{E} and bilinear elements for T took more CPU time than both other methods.

Multimesh hp -FEM vs. single-mesh hp -FEM and multimesh h -FEM, loosely-coupled discretization:

For the sake of completeness, we also introduce results analogous to the previous ones, but with a loosely-coupled discretization which is used much more frequently by practitioners. Now, instead of including the linearized

term $\frac{\tau}{2}\gamma(T_{k-1}^n)\overline{\mathbf{E}_{k-1}^n} \cdot \mathbf{E}_k^n$ from (14) into the stiffness matrix, one simply puts the previous values $\frac{\tau}{2}\gamma(T_{k-1}^n)|\mathbf{E}_{k-1}^n|^2$ on the right-hand side. (This means that the approximate temperature remains real-valued.) As in the monolithic case, we only do one step of the nonlinear iteration per time step.

The approximate solution and meshes for both \mathbf{E} and T were very close to the monolithically coupled case (visually identical to Figs. 5 – 7) and therefore there is no point in showing them. Also the graphs showing the discrete problem size as a function of the physical time, shown in Fig. 12, are almost the same as the ones of the monolithically coupled model shown in Fig. 10.

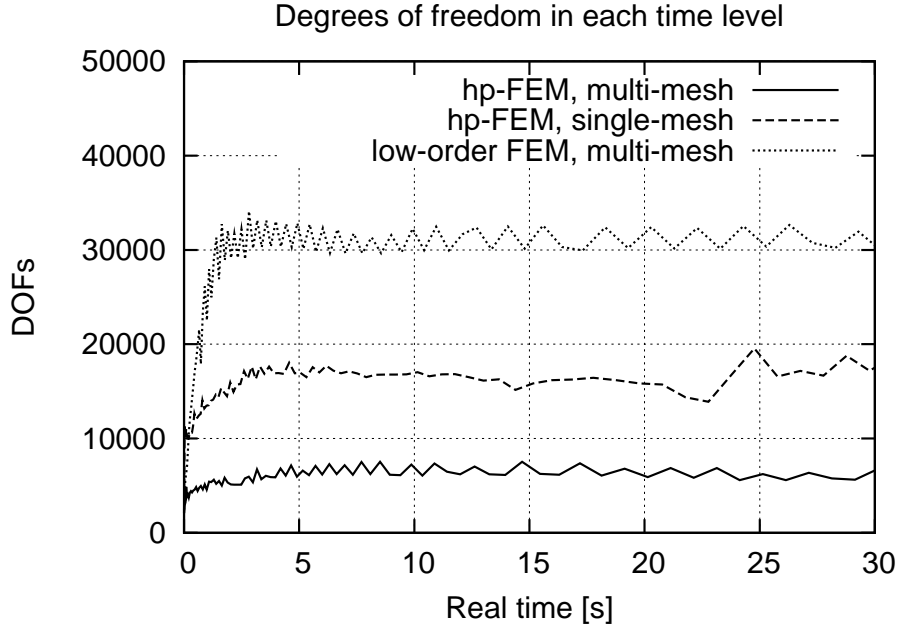


Figure 12: The number of DOF as the function of physical time (loosely coupled discretization).

The following Fig. 13 shows the CPU time of computation as a function of the physical time.

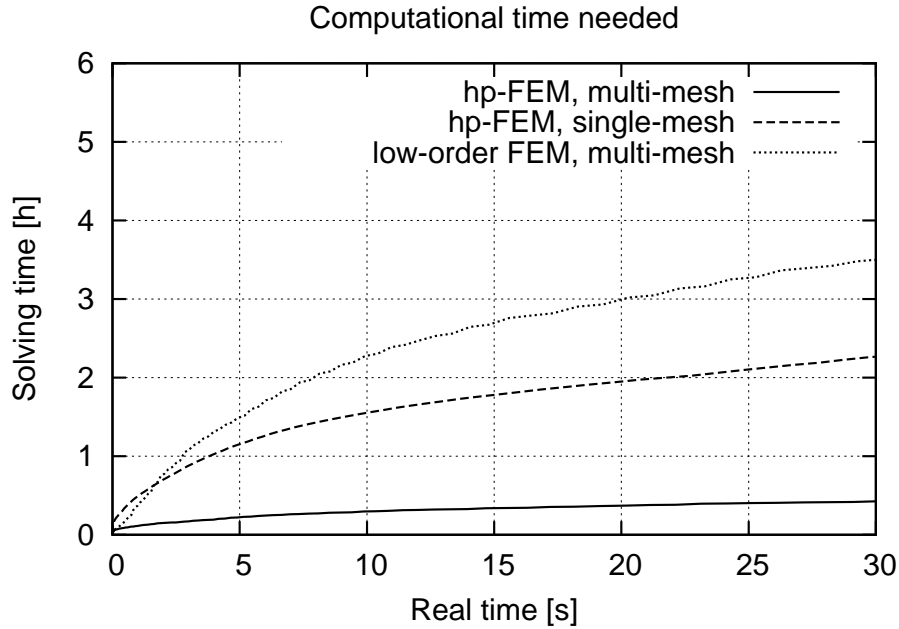


Figure 13: The CPU time of computation as the function of physical time (loosely coupled discretization).

The reader can see that in absolute terms, the loosely coupled computations were approximately twice faster than those in the monolithically coupled case. This is understandable since in the monolithic case more work was required for the assembly of the stiffness matrices and solution of the discrete problems. It follows from Fig. 13 that the space-time adaptive multimesh hp -FEM was the fastest one again, and the low-order FEM remained the slowest as in the monolithically coupled case. In relative terms, the space-time adaptive multimesh hp -FEM was more efficient than the other

two methods, compared to the monolithically coupled model.

5 Conclusions and outlook

We presented a novel version of adaptive hp -FEM suitable for transient microwave heating problems. The method approximates the electric field \mathbf{E} and the temperature T on individual meshes that evolve in time independently of each other, as dictated by the corresponding error components. The automatic adaptivity is guided by a realistic error estimate, not by the residuum or any heuristic criteria such as steep gradients.

To our best knowledge, this is the first paper presenting adaptive hp -FEM for a time-dependent PDE problem. Although \mathbf{E} and T are approximated on different meshes, the discrete problem preserves exactly the coupling structure from the continuous level – in particular, no operator splitting of any kind takes place. The time step is guided adaptively via the so-called PID controller.

By means of suitable numerical experiments we justified the need for adaptive control of the time step as well as the need to approximate \mathbf{E} and T on individual meshes equipped with independent adaptivity mechanisms. We have shown that this is advantageous from the point of view of both the number of DOF (discrete problem size) and the CPU time.

5.1 Future work and open problems

The adaptive strategy described in Paragraph 3.4 is virtually PDE-independent. It was already tested on a number of single- and multiphysics PDE problems, both stationary and transient, always with favorable results. Of course, many particular aspects of the methodology need further elaboration. The most CPU-time consuming part of the algorithm is the repeated assembling of stiffness matrices during the steps of automatic adaptivity. Since only a relatively few refinements take place in every step, many basis functions remain the same and so do their stiffness products. So far we have not taken any advantage of this yet, but we need to do so. Obviously we are aware of multilevel techniques, but their implementation cost is huge and we are not necessarily convinced that they are the best solution to our problem.

Another significant problem that we face is that sparse direct solvers such as UMFPACK cannot handle really large matrices. Iterative solvers are better at this, but we are hesitant to resort to them since we need a matrix solver that works reliably for a wide range of PDE and multiphysics PDE problems. Of course we are aware of various domain decomposition and FETI methods, but we are not completely sure that they are the best we can do. Perhaps a suitable combination of multilevel methods, domain decomposition algorithms, and direct and iterative solvers will be the answer.

Several applications of our novel space and time adaptive hp -FEM to problems such as tracking of interfaces in transient multi-component viscous flow, tracking of shock waves in time-dependent compressible Euler

equations, or evolutionary ideal magnetohydrodynamics are under way. The three-dimensional version of the methodology has been in development now for around five years and we expect to get first concrete results soon.

Last let us mention that the space and time adaptive hp -FEM methodology described in this paper is available in the form of a GPL-licensed modular C++/Python library Hermes. For more details on the open source Hermes project visit the home page of the international hp -FEM group at <http://spilka.math.unr.edu/>. The home page contains various computational videos of space-time adaptive hp -FEM including computations from Section 4.

Acknowledgement

This work was supported by the Grant Agency of the Czech Republic project 102/07/0496, as well as by the Grant Agency of the Academy of Sciences of the Czech Republic project IAA100760702. The research of L. Dubcova was partly supported by the grant No. 48607 of the Grant Agency of the Charles University in Prague.

References

- [1] I. Babuška, W. Gui: The h , p and hp -versions of the finite element method in 1 dimension - Part III. The adaptive hp -version, Numer.

- Math. 49, 659-683, 1986.
- [2] A. Bossavit: Computational Electromagnetism, Academic Press, 1998.
 - [3] T.A. Davis: *Direct Methods for Sparse Linear Systems*, SIAM, Philadelphia, 2006.
 - [4] L. Demkowicz, J. Kurtz, D. Pardo, W. Rachowicz, M. Paszenski, A. Zdunek: Computing with *hp*-Adaptive Finite Elements, Chapman & Hall/CRC Press, 2007.
 - [5] L. Demkowicz, W. Rachowicz, P. Devloo: A Fully Automatic *hp*-Adaptivity. TICAM Report No. 01-28, University of Texas at Austin, 2001.
 - [6] D. D. Dincov, K. A. Parrott: Computational Analysis of Microwave Heating Patterns in Resonant Multimode Cavities. Proceedings of the 2004 ACM Symposium on Applied Computing, 2004, pp. 214–219.
 - [7] P. Kopyt, M. Celuch-Marcysiak: Coupled FDTD-FEM approach to modelling of microwave heating process, Proc. 5th Intern. Conf. on Computation in Electromagnetics (CEM 2004), Stratford-upon-Avon, April 2004.
 - [8] L. Ma, N.M. Potheary, C.J. Railton: Application of the FDTD technique on microwave heating, Computation in Electromagnetics, 1994. Second International Conference on Volume , Issue , 12-14 Apr 1994 Page(s):103 - 106.

- [9] F. Martensen: *The Rothe's Method for Nonlinear Hyperbolic Problems*, Springer, 1986.
- [10] P. Monk: *Finite Element Methods for Maxwell's Equations*, Clarendon Press, Oxford, 2002.
- [11] J.C. Nédélec: Mixed finite elements in \mathbb{R}^3 , Numer. Math. 93 (1980), 315–341.
- [12] R. B. Pandit, S. Prasad: Finite element analysis of microwave heating of potato transient temperature profiles, Journal of Food Engineering, Volume 60, Issue 2, November 2003, Pages 193-202.
- [13] V.M. Puri, R.C. Anantheswaran: The finite element method in food processing: a review, Journal of food engineering 19:33, 247-274, Elsevier, 1993.
- [14] P. Solin, J. Cerveny, I. Dolezel: Arbitrary-Level Hanging Nodes and Automatic Adaptivity in the *hp*-FEM, Math. Comput. Simul 77 (2008), 117 - 132.
- [15] P. Solin, J. Cerveny, L. Dubcova: Adaptive Multi-Mesh *hp*-FEM for Linear Thermoelasticity, Research Report No. 2007-08, Department of Mathematical Sciences, University of Texas at El Paso, <http://www.math.utep.edu/preprints>, submitted to J. Comput. Appl. Math.

- [16] P. Solin, L. Dubcova, J. Cervený, I. Doležel: Adaptive hp -FEM with Arbitrary-Level Hanging Nodes for Maxwell's Equations, submitted to Math. Comput. Simul.
- [17] P. Solin, K. Segeth, I. Doležel: *Higher-Order Finite Element Methods*, Chapman & Hall/CRC Press, 2003.
- [18] A. M. P. Valli, G. F. Carey and A. L. G. A. Coutinho: Control strategies for timestep selection in simulation of coupled viscous flow and heat transfer. Commun. Numer. Methods Eng. 18 (2002), no.2, 131-139.